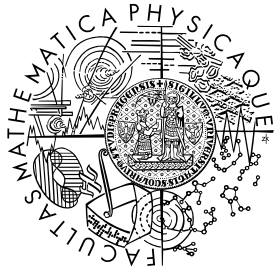

FACULTY
OF MATHEMATICS
AND PHYSICS
Charles University

BACHELOR THESIS

Karel Balej

Monte-Carlo simulation of background in the reactor antineutrino detector NuGeN

Institute of Particle and Nuclear Physics

Supervisor of the bachelor thesis: Ing. Vít Vorobel, Ph.D.
Consultant: Ing. Karel Smolek, Ph.D.
Study programme: Physics
Study branch: General physics

Prague 2022

I declare that I carried out this bachelor thesis independently, and only with the cited sources, literature and other professional sources. It has not been used to obtain another or the same degree.

I understand that my work relates to the rights and obligations under the Act No. 121/2000 Sb., the Copyright Act, as amended, in particular the fact that the Charles University has the right to conclude a license agreement on the use of this work as a school work pursuant to Section 60 subsection 1 of the Copyright Act.

In ..... date ....

Author's signature

I thank to Karel Smolek for his professional guidance and friendly approach and also to Vít Vorobel not only for agreeing to supervise this thesis but also for investing so much time in it. My thanks also belong to Alexey Lubashevskiy and other members of the νGeN team for welcoming us so kindly at their institute and for allowing me to use some of their materials in the thesis. I am also grateful to Michal Jireš for helping me identify bugs in my program and my roommates for their patient explanation of various C++ concepts. Last but not least, I thank to Petr and Radek Olšák for their advice regarding the usage of OpTEX and quick resolution of any issues that I encountered.

Title: Monte-Carlo simulation of background in the reactor antineutrino detector NuGeN

Author: Karel Balej

Department: Institute of Particle and Nuclear Physics

Supervisor: Ing. Vít Vorobel, Ph.D., Institute of Particle and Nuclear Physics

Consultant: Ing. Karel Smolek, Ph.D., Institute of Experimental and Applied Physics, Czech Technical University in Prague

Abstract: This thesis aims to analyze the influence of the neutron background of a nuclear reactor on measurement of the νGeN experiment which is placed underneath it. This experiment is designed for detection of the CEνNS (coherent elastic neutrino-nucleus scattering). A simulation of the neutron spectrum based on an on-site measurement is performed using the GEANT4 framework. The results are then compared with the expected CEνNS signal and the first measurements of the experiment and discussion is carried out regarding its role and the effect of the experiment shielding.

Keywords: Monte-Carlo, neutrino, HPGe detector

Table of contents

Introduction

The νGeN [1, 2] experiment's main objective is the detection of the coherent elastic neutrino-nucleus scattering (CEνNS) of low energy neutrinos ($E_\nu < 50$ MeV)

$$\nu + \mathrm{A} \rightarrow \nu + \mathrm{A}.$$

This is an interaction allowed within the Standard Model with a fairly large cross-section making its detection possible with table-top sized detectors which would open new ways for studying these arguably least understood particles of the Standard Model. Aside from being very practical for neutrino research it also implies many new possibilities for neutrino-based applied research, such as non-intrusive monitoring of nuclear reactors.

Reactor antineutrinos produced by the reactor of the Kalinin Nuclear Power Plant are used for the experiment as nuclear power reactors generate the largest neutrino flux of all artificial neutrino sources. Neutrinos produced in reactors also have energies less than 50 MeV and thus they are suitable for the coherent scattering interaction with nuclei of atoms.

While CEνNS has a comparatively large cross-section, it is still extremely difficult to detect it, because the only evidence it leaves is a nuclear recoil the energy of which, however, is very small. Therefore in order to be able to draw relevant conclusions from results of an analysis of experimental data two main matters must be considered first. The first one being an estimation of the expected number of events in the energetic region of interest (ROI), the other one being an assessment of background which burdens the experiment and its comparison with the expected signal from CEνNS.

Discussion of the latter of these will be the main goal of this thesis. There are several sources of background affecting the experiment. The focus will be narrowed here only to the background caused by neutrons from the reactor. Thus, any other sources will be neglected and it will be assumed that all the neutrons appearing in the detector room come from the reactor and the environment around it.

1 Theory

1.1 Neutrino

Neutrino [3, 4] is a particle first proposed by Wolfgang Pauli in 1930 in order to save the law of conservation of energy, which seemed to be violated in the beta decay

$$\mathrm{A} \rightarrow \mathrm{B} + e^{-},$$

where nucleus A is transformed into nucleus B while an electron e^{-} is emitted. Here, the laws of kinematics predict a fixed energy for the emitted electron, which however is not what was observed – the observed energy varied significantly. Pauli explained this by introducing a new particle, which had to have zero electric charge (in order not to violate the law of conservation of charge instead) and which carried off the energetic difference in the beta decay. With the discovery of neutron two years later, the process could be schematically amended as follows:

$$n \rightarrow p^{+} + e^{-} + \bar{\nu}_{e}, \tag{1.1.1}$$

where n stands for neutron, p for proton and $\bar{\nu}_{e}$ is now recognized as an electron antineutrino (as the terminology later embraced new findings).

As a consequence of the electron energies in the beta decay ranging up to the kinematically predicted energy it was deduced, that the neutrino must be very light, originally it was even thought to have zero rest mass – it was later shown that this should not be the case and the current upper limit is determined by the KATRIN experiment as 0.8 eV$\cdot c^{-2}$ [5]. The reason for this was first theorized by Bruno Pontecorvo [6, 7] in 1957. Based on the expectation of more types of neutrino (which was however not confirmed yet at the time), he suggested a mechanism of neutrino oscillation and mixing. The basic idea says that neutrinos exist in eigenstates of mass and flavor and evolve between these states. Neutrino oscillation was then first witnessed in 1998 by the Super-Kamiokande experiment [8] in Japan and conclusively confirmed in 2001 by the SNO experiment [9] in Canada which solved the long lasting solar neutrino problem – the theoretical amount of electron neutrinos coming from the Sun did not correspond to the actual amount measured. This was because approximately two thirds of them changed their flavor on the way from the Sun to the Earth and became muon or tau neutrinos.

Solar neutrinos are produced in fusion processes in the Sun and are always of the electron flavor. They are useful for instance for the study of the Sun's core because due to their inertness, they leave the Sun more easily and reach the Earth sooner than photons. Beside the Sun, there are other notable sources of (anti)neutrinos. Majority of muon neutrinos and antineutrinos on Earth comes from the interaction of cosmic radiation with the upper parts of Earth's atmosphere. Here, a cascade of particles is produced eventually yielding muon antineutrinos and muons (or muon neutrinos and antimuons) which often further decay to electron, electron antineutrino and muon antineutrino. Just as with solar neutrinos, there was a discrepancy between the expected amount of muon neutrinos and

the amount observed in experiments[1]. This problem was again explained by the neutrino oscillation phenomenon.

Reactor neutrinos were the first ones to be observed in 1956 in a Los Alamos experiment called *Project Poltergeist* [10] – the name of the experiment refers to the fact, that since neutrino is very light and interacts very rarely and weakly (they are only affected by the gravitational and weak interactions), it is immensely difficult to detect it, like a ghost. That's why it is necessary to construct huge detectors in order to detect them – for comparison, the Los Alamos detector weighed ten tons – big detectors increase the probability that the neutrino will interact and leave some kind of trace. Another way to increase this chance is to have a strong source that produces large quantities of neutrinos – on Earth these are most notably the nuclear reactors which provide an intense, steady and well-defined (just one type of neutrino is produced here) flux of electron antineutrinos born in the beta decay in the reactor. With these properties, nuclear reactors constitute the most important neutrino source for research purposes. Detectors can also be placed in various distances from reactors which allows for the study of neutrino oscillation over various spatial intervals.

In 2011, an article [11] was published in which the authors pointed out an experimental deviation from the theoretically expected reactor antineutrino flux – a discrepancy which they called the *reactor antineutrino anomaly*. They also hypothesized and discussed the possibility of the anomaly being caused by the existence of the fourth neutrino flavor emerging as a result of a very short baseline neutrino oscillation. This fourth flavor is called *sterile* because it is thought to only interact via the gravitational interaction (unlike regular neutrinos, which are, besides gravity, also susceptible to the weak interaction) causing it to be even more difficult to observe due to its low mass. Following these considerations, new experiments looking for the sterile neutrino were launched, such as the DANSS experiment [12] at the Kalinin Nuclear Power Plant in Russia.

1.1.1 CEνNS

Coherent elastic neutrino-nucleus scattering [13] is a particular mode of interaction of neutrinos with atomic nuclei first predicted by Daniel Z. Freedman in 1974 [14]. In this process, a neutrino, independently of its flavor, interacts with the entire nucleus at the same time by exchanging the Z^0 boson with all of its nucleons (refer to Fig. 1.1.1). This coherence results in the interaction having a large cross-section, which can be calculated by integrating the differential cross-section [15]

$$\frac{\mathrm{d}\sigma_{\mathrm{CE}\nu\mathrm{NS}}}{\mathrm{d}T} = \frac{G_F^2 M Q_W^2}{4\pi}\left(1 - \frac{MT}{2E_\nu^2}\right) F^2(Q^2), \tag{1.1.2}$$

where $Q_W = N - (1 - 4\sin^2\theta_W)Z$ is the weak charge, θ_W the Weinberg angle, N the number of neutrons in the target nucleus, Z the number of protons, T the recoil energy, E_ν the neutrino energy, M the mass of the target, $Q = \sqrt{2 - 2\cos\theta}E_\nu$ the transferred momentum, θ the scattering angle, G_F the Fermi constant and $F(Q^2) \propto \exp -\frac{R^2Q^2}{6}$ (R being the nucleus radius) the elastic nuclear form-factor. This has the important benefit that the detectors can be table-top sized in contrast to the gigantic devices necessary in order to detect neutrino interactions

[1] More precisely the inconsistency was in the ratio of muon neutrinos and antineutrinos to electron neutrinos and antineutrinos, which were expected to make up about one third of the neutrinos born in the atmosphere.

via different channels – this has many advantages for neutrino research, but it also opens door to industrial applications, for instance it could be taken advantage of for non-intrusive monitoring of nuclear reactors. Yet, it has taken over four decades until this phenomenon was first observed experimentally by the COHERENT collaboration [16] – that is because of the nature of the interaction: the neutrino scatters elastically on the much heavier nucleus causing its recoil (refer to Fig. 1.1.2), however due to the many orders of magnitude of difference in mass between the two objects, the energy of this recoil transmitted from the neutrino to the nucleus is very low and so very sensitive and precise detectors and a low background are needed to make the detection possible.

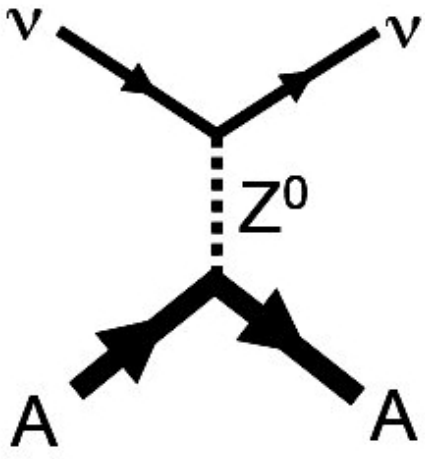

Figure 1.1.1 Coherent elastic neutrino-nucleus scattering [1].

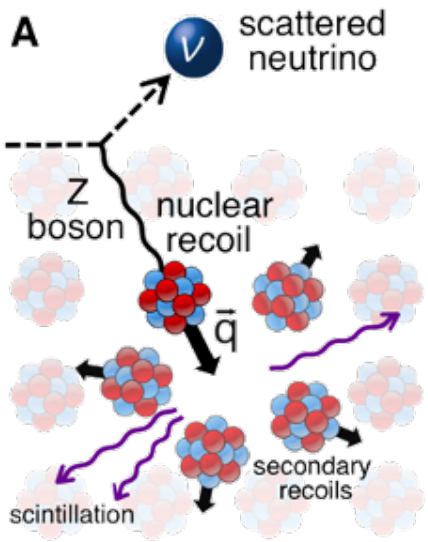

Figure 1.1.2 Nuclear recoil of CEνNS [13].

1.2 νGeN

The νGeN experiment [1, 2] was started at the Joint Institute for Nuclear Research [17] in Russia with the goal of detecting CEνNS (refer to Sec. 1.1.1). The neutrinos used by the experiment come from a reactor at the Kalinin Nuclear Power Plant (KNPP) in Udomlya, Tver Region, Russia. There, a high purity germanium (HPGe) detector is located in a special chamber under the nuclear

reactor of unit number 3. The detector performs measurements both with the reactor on and off. To mitigate systematic errors connected with changes in background caused by this, the detector is installed on a special lifting mechanism (see Fig. 1.2.1) which allows for an alteration of the neutrino flux through the detector. The mechanism allows the detector to move between 10.869 and 11.935 meters from the center of the reactor core.

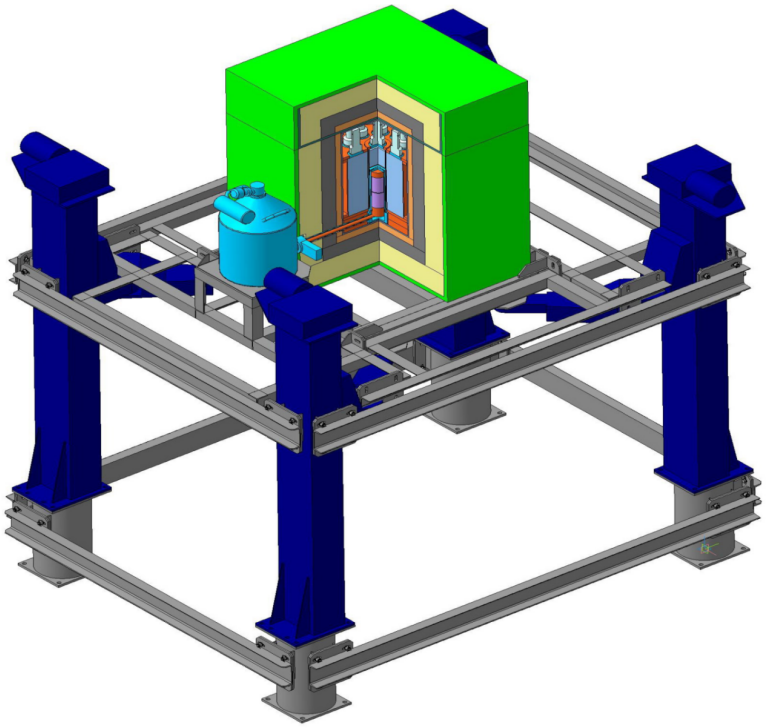

Figure 1.2.1 Schema of the detector lifting mechanism [1].

1.2.1 Detector construction

Based on the schemes[2] provided by the detector manufacturer, the Mirion Technologies company [18], the main component of the custom-designed low threshold detector is a cylindrical crystal made of high purity germanium (HPGe) with 70 mm in diameter and in height and it weighs 1.41 kg. This is surrounded by an inner case of aluminum alloy and placed onto an insulator which is supported by a cylindrical base made of copper. To this, a cooling pipe is attached at the bottom. The pipe consists of an inner copper tube and an aluminum cover. Through it, the detector is connected to a cooling device. Four detectors were manufactured in total, each with one of two types of the cooling system: either electric or nitrogen based. Both types are shown in Fig. 1.2.2. The outside of the detector is plated with aluminum.

The detector is shielded by several layers of material to suppress gamma and neutron background. The innermost layer covering the device, which is enclosed in an aluminum shell, is made of a 3D printed nylon. This is split into blocks with cylindrical cutout in the middle as is depicted in the drawing in Fig. 1.2.3. Those are then stacked onto each other to cover the full height of the aluminum shell. Around this, 10 centimeters thick walls made of oxygen free copper bricks are built, followed by a layer of 3.5 % borated polyethylene. Next, the setup is surrounded by a layer of lead, which is again followed by the 3.5 % borated

[2] The schemes are of a proprietary character and thus it was not possible to include them.

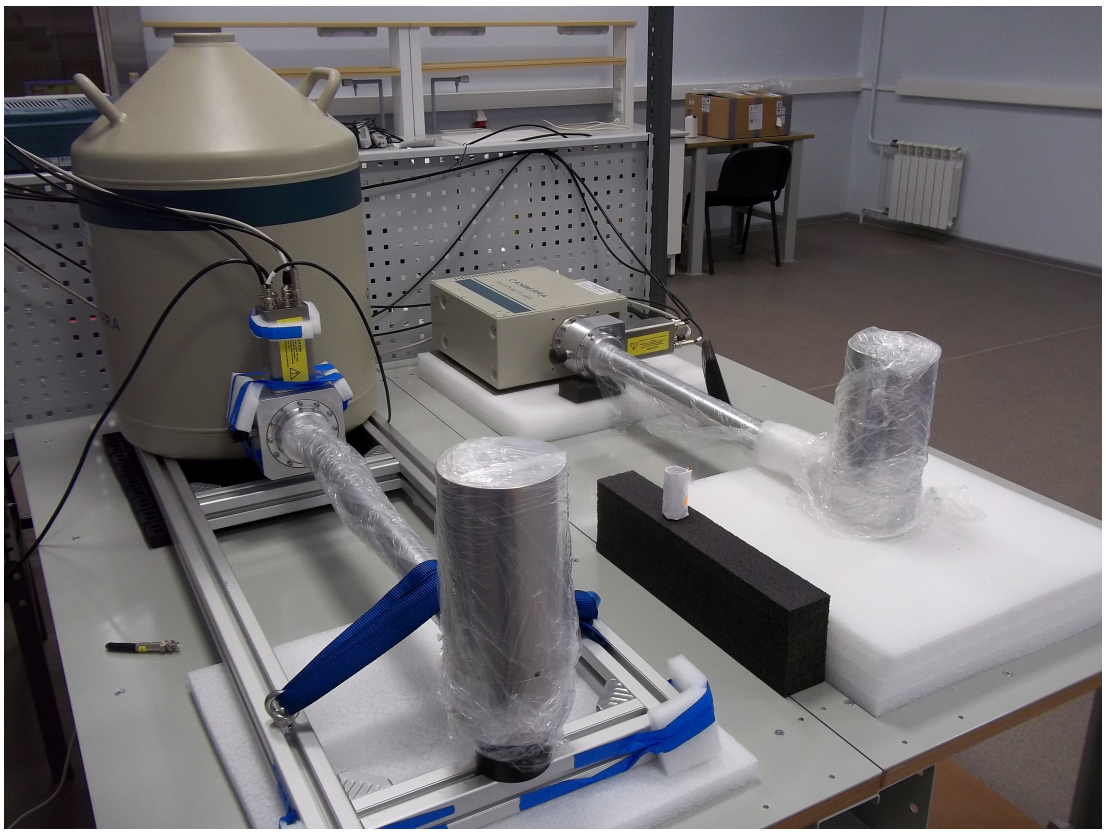

Figure 1.2.2 The detector used for the νGeN experiment together with the two types of cooling.

polyethylene. Outer layer is an active muon veto made of polystyrene. Schematic depiction of the shielding setup from which also thickness of each layer can be read can be found in Fig. 1.2.4.

1.2.2 First measurements

Extensive calibration of the detector has been performed and at the end of 2019 it has been installed in the detector room under the KNPP reactor with the electric cooling device. In December 2020, an antivibration system intended to suppress the microphonic effect was added and the data collection began during which the reactor was off for about sixty days. Stable event rate was observed during the entire time. The distance of the detector from the reactor center was 11.835 m, where the antineutrino flux has been estimated to be $3.9 \cdot 10^{13}$ cm^{-2}·s^{-1} [2]. The collected data is shown in Fig. 1.2.5 – days with zero rates were dedicated to further calibration. Comparison of the data and the expected signal, which was calculated using Eq. (1.1.2) based on the estimated antineutrino flux at the given distance from the reactor, is presented in Fig. 1.2.6. A region of interest (ROI) has been chosen as $\langle 320, 360 \rangle$ eV as there the ratio of expectation to data is the largest and low energy noises are not present. There, 2.32 ± 0.15 events per day per kilogram were seen for the reactor on and 2.34 ± 0.21 events per day per kilogram with the reactor off, whereas the expected contribution from CEνNS with the quenching factor 0.179 is 0.43 events per day per kilogram [2]. In Fig. 1.2.7, the difference of observed events with the reactor on and off is plotted along with the expected CEνNS signal – no significant difference expected to be contributed by CEνNS can be seen between these two regimes of the reactor and so no observation of CEνNS has been made so far.

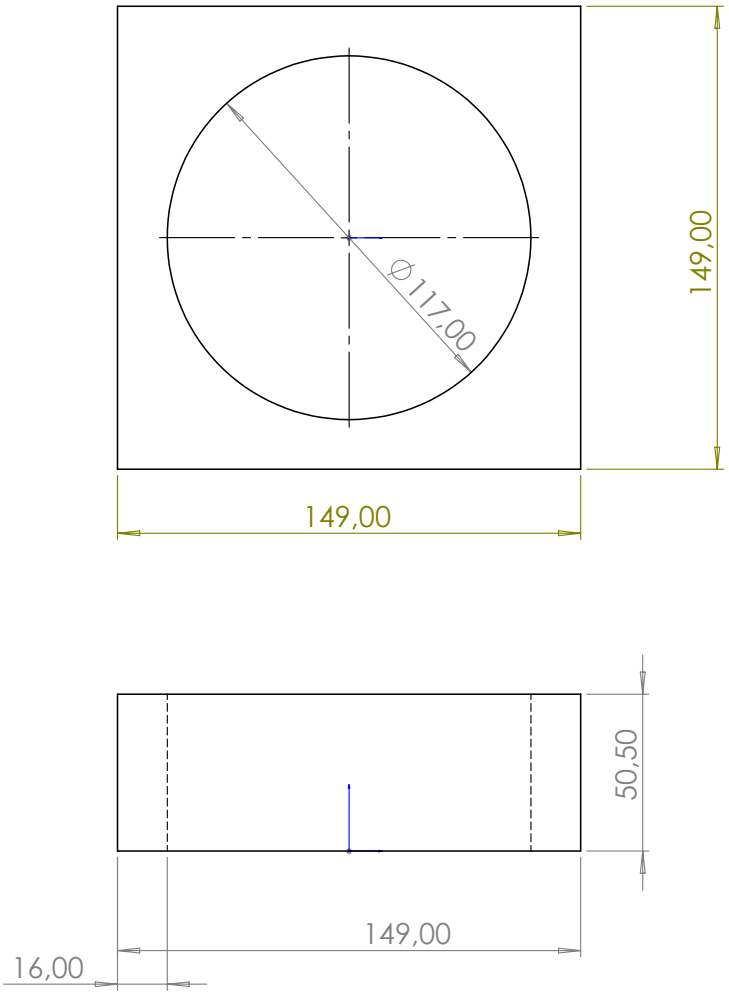

Figure 1.2.3 The dimensions of the nylon shielding blocks, top and side view (image courtesy of Konstantin Shakhov).

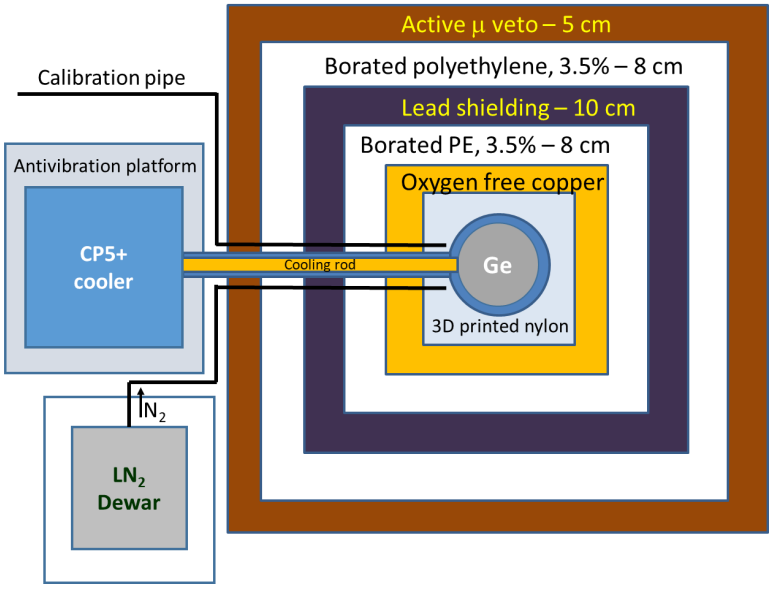

Figure 1.2.4 Schema of the shielding construction [2].

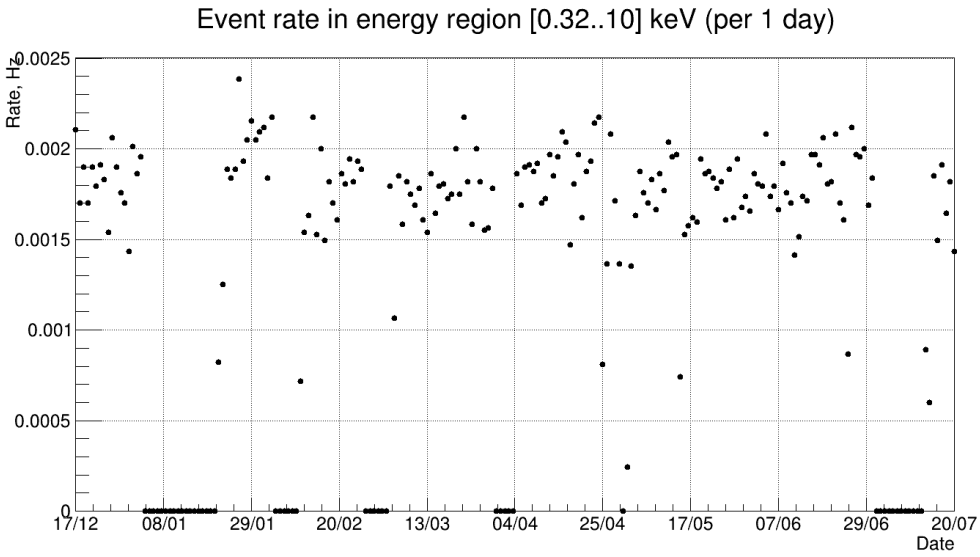

Figure 1.2.5 Data collected during the first νGeN measurement (graph courtesy of the νGeN team).

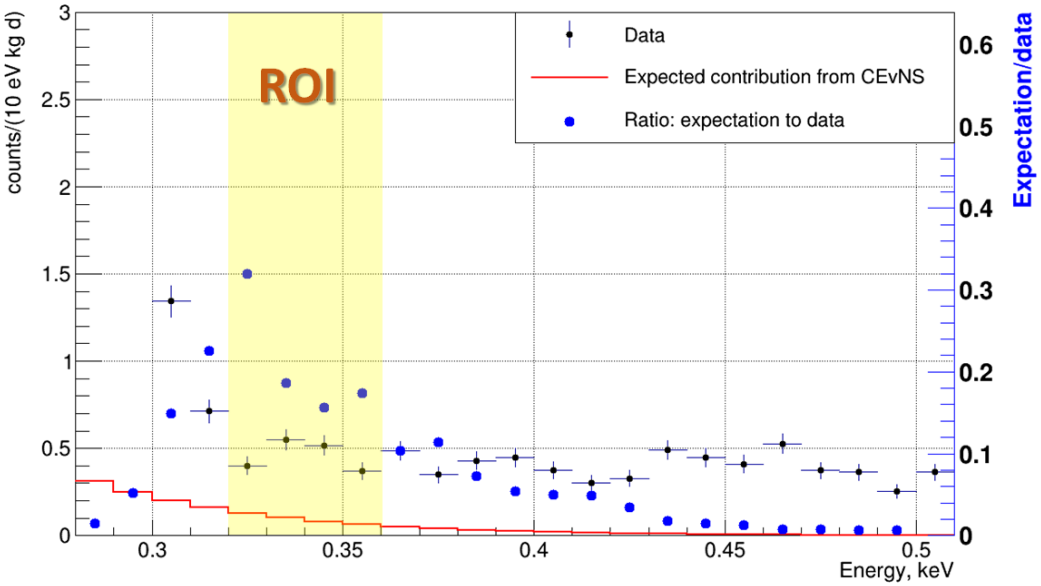

Figure 1.2.6 Comparison of the measured data and the theoretically expected signal from CEνNS [2].

1.3 Interaction of neutrons with matter

Neutrons, discovered by James Chadwick in 1932 [19], are particles similar to protons – they have nearly the same mass and together with them they form nuclei of atoms, which is why they are collectively called nucleons. Just as protons, they consist of quarks which are bound by the strong interaction via gluons, specifically two down quarks and one up quark, whereas protons are made up of two up quarks and one down quark – this is the reason why neutrons have no electric charge while protons do, as up and down quarks have a fractional charge of $\frac{2}{3}e$ and $-\frac{1}{3}e$ respectively, where e is the elementary charge. Together they constitute the majority of atomic mass and hence the mass of all matter. Unlike a free proton, a free neutron is unstable and decays into proton, electron and

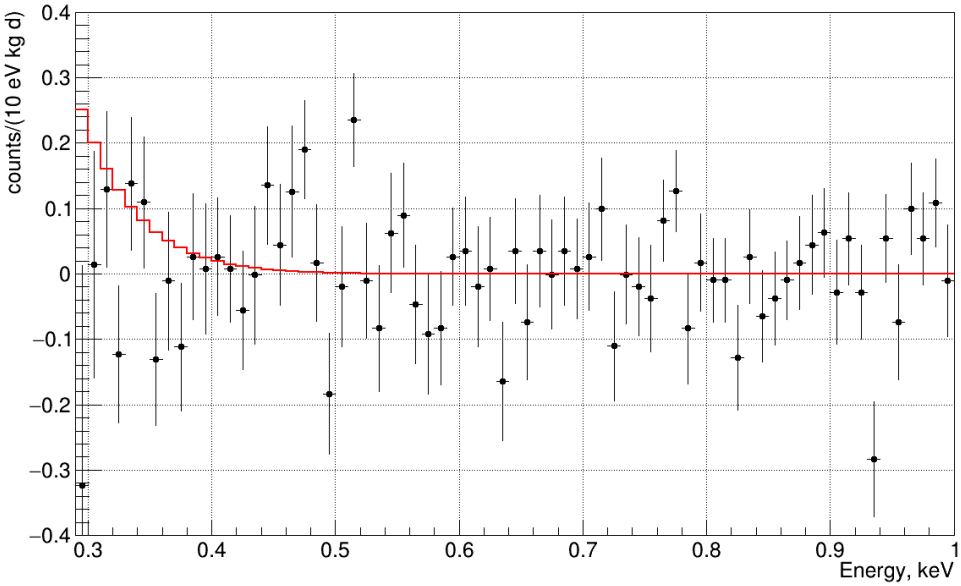

Figure 1.2.7 Difference of the event count with the reactor on and off along with the expected CEνNS signal [2].

electron antineutrino in the beta decay (see Eq. (1.1.1)), which is only possible because the neutron has slightly more mass than the proton.

By their energy, free neutrons can be classified into several types. Neutrons with energies greater than 100 keV are usually denoted as fast [20], the range between 10 eV and 100 keV is designated as intermediate neutrons and energies below 10 eV belong to slow neutrons. Thermal neutrons is a term for neutrons, which are approximately in a thermal equilibrium with the environment. The energy distribution can then be assumed to be approximately Maxwell-Boltzmannian and from this the most probable energy can be determined as $E \approx 0.025$ eV [21] at the room temperature $T \approx 300$ K. At these energies, neutrons exhibit a gas-like behavior [22].

As neutrons have no charge, they interact primarily via collisions [20]. During elastic scattering, the energy is conserved and the neutron bounces off the target. The energy transferred to the target depends on the angle under which the neutron bounces. Elastic scattering is the most probable interaction for most targets and neutron energies and forms the basic principle of neutron moderators. In an inelastic scattering, some energy is lost to the excitation of the target nucleus, which then emits a photon as it deexcites. Because there is a threshold energy needed for the excitation of the nucleus, inelastic scattering does not occur for neutrons with a lower energy. Neutrons can also be captured by the target nucleus. This can lead to an emission of some other particle, such as a proton, and if the nucleus is left excited after the interaction, it may also release a gamma photon while returning to its ground state. Depending on whether there is a threshold energy for the neutron, the reaction can either be exothermic (no energy required) or endothermic (some minimal energy must be carried by the neutron in order to activate the reaction). The cross-section of all these interactions depends on the type of the target and the neutron energy. The neutron capture is most likely with thermal neutrons.

These processes are taken advantage of for moderator and shielding design. The principle of a neutron shielding is usually as follows [20]. First, a moderator

is used to slow the neutrons down. Nuclear power plants are known to utilize water for the moderation of neutrons, while for research applications plastic is often used. Sometimes, iron or lead is used to slow down neutrons with very high energies – in the case of lead, this generates gammas with energies of 0.8 MeV and 2.6 MeV [23]. After neutrons are sufficiently slowed down, which increases the probability of their interaction via capture, they are passed through some hydrogenous material so that they are absorbed. Hydrogen captures neutrons in the reaction

$$n + {}^{1}\mathrm{H} \rightarrow {}^{2}\mathrm{H} + \gamma, \tag{1.3.1}$$

where the gamma photon carries off the energy of 2.2 MeV. Boron is often mixed in because of the large cross-section of the neutron-boron capture and low energy of the gammas produced [24]:

$$n + {}^{10}\mathrm{B} \rightarrow {}^{4}\alpha + {}^{7}\mathrm{Li} + (0.477\ \mathrm{MeV})\gamma. \tag{1.3.2}$$

Hydrocarbons are often utilized, where neutron-carbon interaction additionally produces 4.4 MeV photons [23]. Thus produced gammas are then absorbed by a high density material with a high atomic number [25].

1.4 Software

1.4.1 GEANT4[3]

GEANT4 [26, 27, 28] is a particle physics simulation toolkit developed by a worldwide collaboration of scientists and software engineers. It aims to simulate the passing of particles through matter and their interaction. For this purpose, it utilizes the Monte Carlo method [29] which employs probabilistic approach to evaluate in principle deterministic but complicated situations. As such it relies on a generation of random numbers, these however need not be truly random and a pseudo-random generator can be used (just as is in GEANT4), which is in fact often desirable in order to be able to reproduce certain results. Implemented as a C++ library, the toolkit uses object oriented programming to enable the user to have a full control over the simulation. User is required to define several mandatory components: the detector geometry, particles and physics processes which should be simulated and the generation of primary events. The simulation itself runs in small steps during which all physical processes relevant to the given particle are evaluated with the Monte Carlo method. Various information about the steps is available, such as the pre-step and post-step position or the total energy deposited during the step.

1.4.2 ROOT

ROOT [30] is a data analysis framework created at CERN (European Organization for Nuclear Research). It provides statistical and mathematical tools for data evaluation, including creating histograms and plotting graphs. It also enables users to store the data in a native binary format designed for fast access which can among others be taken advantage of for experiments which produce large amounts of data, such as the Large Hadron Collider where it was among other things utilized in the discovery of the Higgs boson. Another prominent feature of ROOT is that besides being compiled into a program, it can also be launched

[3] Version 11.0.0 of GEANT4 was used for this thesis.

interactively or execute macros from files. ROOT exposes bindings which allow for its native use in other programming languages besides C++, in which and for which it is primarily written, such as PYTHON or R.

2 Simulation

2.1 Model of the experiment

The geometry of the experiment was modeled based on the information described in Sec. 1.2.1 using the tools provided by the GEANT4 framework. Several approximations and simplifications were considered especially with regard to the inner structure of the detector, due to the unclarity of some of the provided schemes presented by the νGeN team but also to simplify the construction where it was believed that it would not have any significant effect on the output of the simulation. The most notable simplification outside of the detector was the omission of the pipe connecting it to the cooling device.

In GEANT4, volumes constitute a hierarchy where daughter volumes are placed inside a mother volume which they appropriately overwrite. The outermost and main volume is called *World* and all other volumes are placed therein. The detector was modeled as an aluminum cylinder. Into this, a cylindrical cavity of vacuum[4] was placed in accordance with the described thickness of the outer aluminum shell. There, the HPGe crystal was put as a cylinder of appropriate dimensions (refer to Sec. 1.2.1) surrounded by an inner case of aluminum. Below the crystal, a disk of copper was placed followed by an insulation disk of polytetrafluoroethylene (PTFE). This was then connected through a cascade of copper cylinders to a leg of the cooling pipe, modeled as a copper tube enclosed in a hollow pipe of a thin layer of aluminum. For a visualization of the model generated by the GEANT4 visualization driver refer to Fig. 2.1.1.

The various layers of shielding were represented by boxes, each made of the appropriate material. These were then stacked into each other following the shielding hierarchy described in Sec. 1.2.1. Into the innermost box of nylon, the detector was placed, meaning that no gap between the detector and the shielding implied by their respective dimensions was inserted. The visualization of the full setup of the simulation is presented in Fig. 2.1.2. The muon veto was modeled as polystyrene.

Where applicable, materials internally constructed by GEANT4 were utilized (muon veto: `G4_POLYSTYRENE`, polytetrafluoroethylene: `G4_TEFLON`, germanium: `G4_Ge`, copper: `G4_Cu`, aluminum: `G4_Al`, nylon: `G4_NYLON-6-6`) with the exception of borated polyethylene. This was constructed manually from appropriate chemical elements based on a common chemical composition of neutron shielding [31] as a mixture of polyethylene CH_2 and boric acid H_3BO_3 in a way so that 3.5 % of the mass of the resulting compound was made up of boron: molar mass of boron 10.81 grams, of boric acid 61.83 grams [32], hence boric acid should constitute $x = \frac{61.83}{10.81} \cdot 3.5\ \%$ of mass of the resulting material. Density of the mixture was calculated from the reciprocal relation

$$\frac{1}{\rho_{CH_2+H_3BO_3}} = \frac{1-x}{\rho_{CH_2}} + \frac{x}{\rho_{H_3BO_3}}.$$

Supposing $\rho_{CH_2} \approx 0.94$ g/ml and $\rho_{H_3BO_3} \approx 1.44$ g/ml [32], a value of $\rho_{CH_2+H_3BO_3} \approx 1$ g/ml is obtained.

[4] In GEANT4 (as in the real world), there is no such thing as vacuum and hence it is approximated by a very low density gas (`G4_Galactic`) in the simulation.

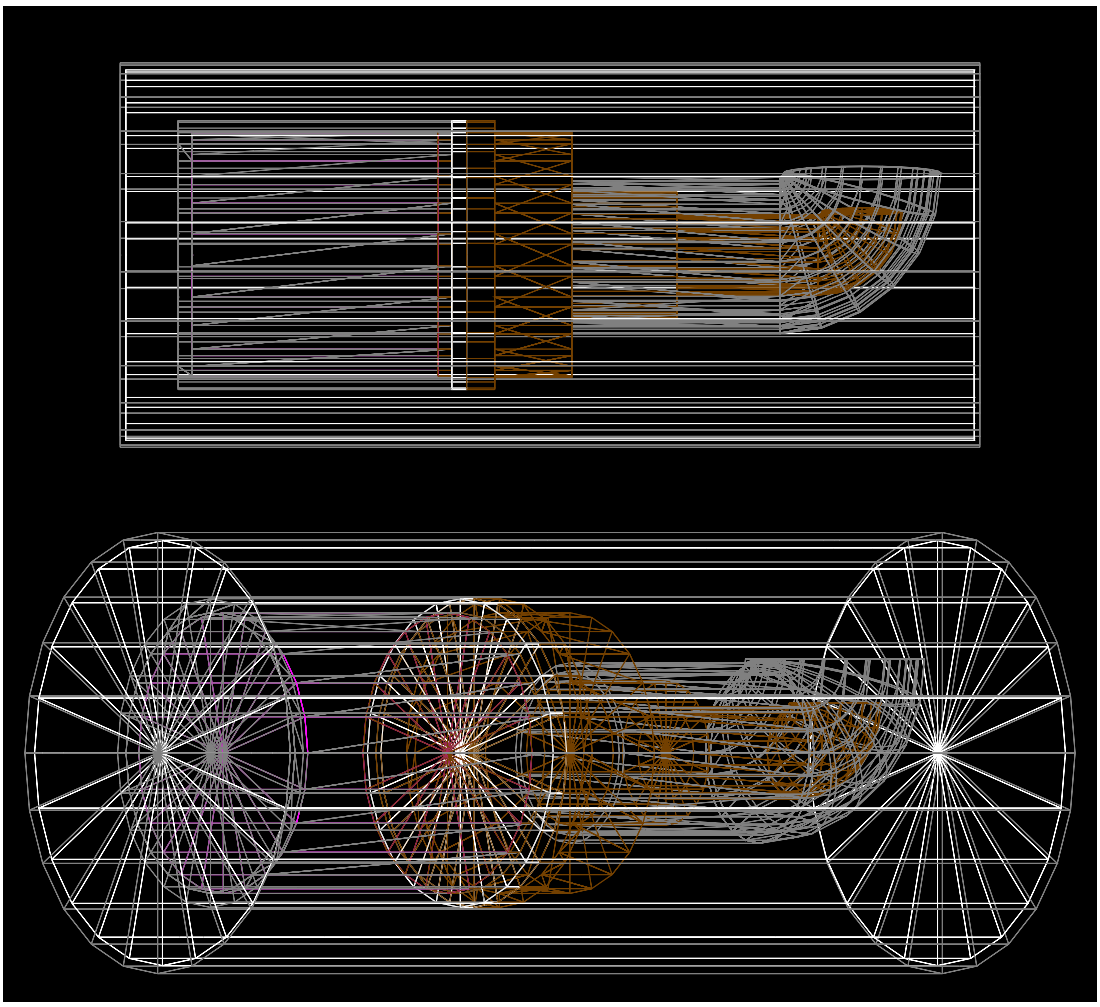

Figure 2.1.1 Visualization of the detector as generated by the GEANT4 visualization driver (side and corner views) – in the image, volumes of aluminum are colored gray, volumes of copper are brown, PTFE is white and germanium is magenta.

2.2 Input neutron spectrum

Spectrum used for the generation of the primary events in the simulation was based on an on-site measurement performed by the νGeN team in the detector chamber under the reactor in the KNPP. A ^{3}He detector was placed on top of the outermost layer of shielding of the νGeN detector for the duration of thirty days, half of which the reactor was on and half off – only the spectrum obtained with the reactor on was considered and it is plotted in Fig. 2.2.1. Unfolding of this spectrum and estimation of the real neutron flux around the experiment was performed by Ing. Karel Smolek, Ph.D. The reaction occurring in the helium detector is

$$n + {}^3\mathrm{He} \rightarrow p + {}^3\mathrm{H}, \tag{2.2.1}$$

where the sum of energies of proton and triton is 764 keV plus the kinetic energy of the neutron. Thence the entire spectrum from Fig. 2.2.1 was shifted by 764 keV – the difference of the detected energy of the reaction products and the minimal energy of 764 keV was caused by the energy transferred by the interacting neutron. Special treatment was applied to thermal neutrons, where it was assumed, based on an analysis of results of a similar measurement [33] performed in the LSM [34], that thermal neutrons make up a portion of the peak around 764 keV (see

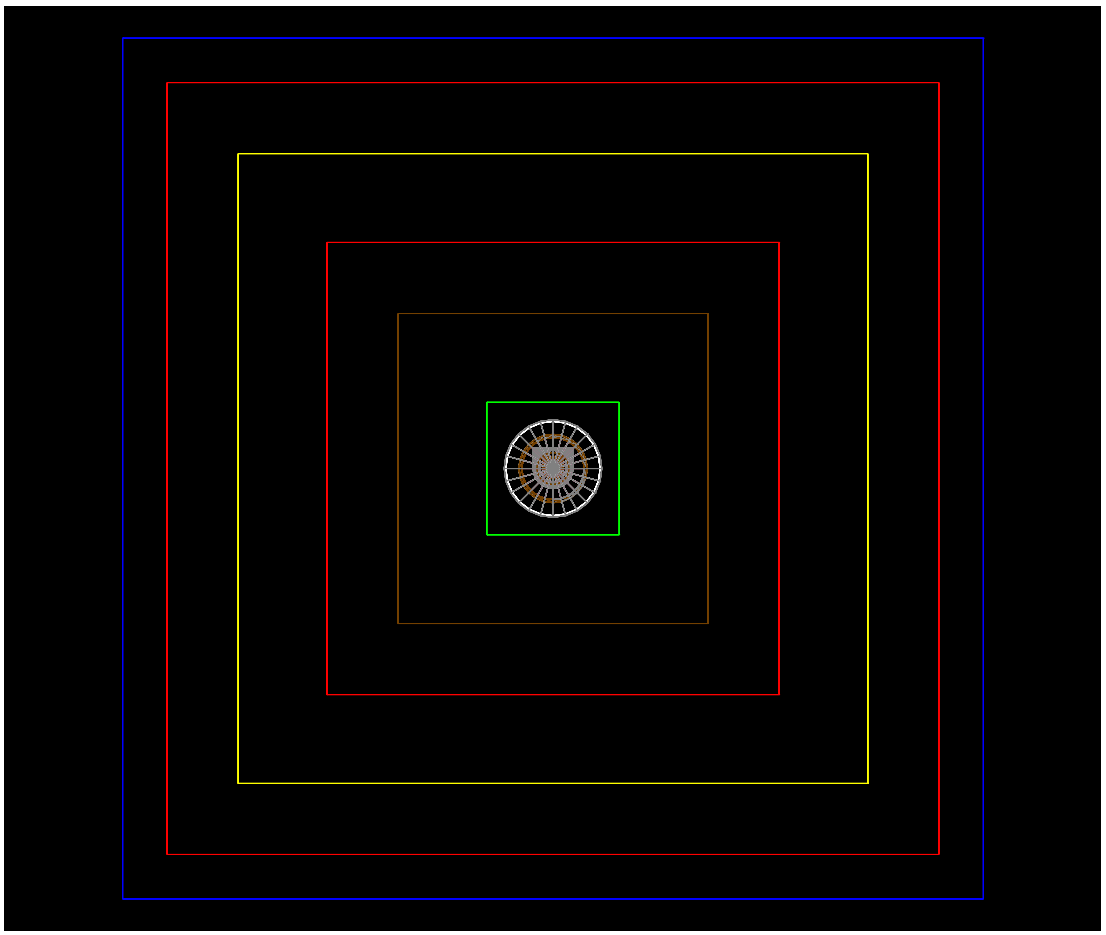

Figure 2.1.2 Visualization of the simulation setup, top view – green color corresponds to nylon, blue to polystyrene, red to polyethylene and yellow to lead, other colors are the same as in Fig. 2.1.1.

Fig. 2.2.2) in the region from 660 keV to 830 keV (with respect to the original spectrum). These events were hence added together and attributed to thermal neutrons with an energy of 0.025 eV[5]. Such spectrum was then reweighed by the reciprocal of the cross-section of the interaction described in Eq. (2.2.1) obtained from the BNL database [35]. Thus an estimate of the relative spectrum was made.

The absolute flux, which is necessary in order to scale the simulation results to time, was estimated again with the use of the LSM paper [33]. One neutron per centimeter squared of the real flux was assumed to correspond to 243 detected events in the region of thermal neutrons. After division by the time of the measurement, the absolute flux was determined to be 79 neutrons per $\mathrm{m}^2{\cdot}\mathrm{s}$ for thermal neutrons and 274 neutrons per $\mathrm{m}^2{\cdot}\mathrm{s}$ for higher energy neutrons. The final spectrum can be seen in Fig. 2.2.3 – the formula for count in each bin is

$$\mathrm{bin}(E) = \mathrm{bin}_{\mathrm{measured}}(E + 764\ \mathrm{keV})\frac{\sigma(0.025\ \mathrm{eV})}{\sigma(E)}\frac{1}{243 \cdot 10^4 \cdot 1.3 \cdot 10^6}\mathrm{m}^{-2} \cdot \mathrm{s}^{-1},$$

where E is the energy of the given bin and σ the cross-section of the interaction for a neutron with the given energy. As the helium detector was placed on the experiment shield, this flux was assumed to originate in one half-space. For the simulation, to approximate the gas-like behavior of thermal neutrons (see

[5] As was discussed in Sec. 1.3, the distribution of energies here should be Maxwellian, this was however neglected as it was not believed to be of high relevance to this simulation.

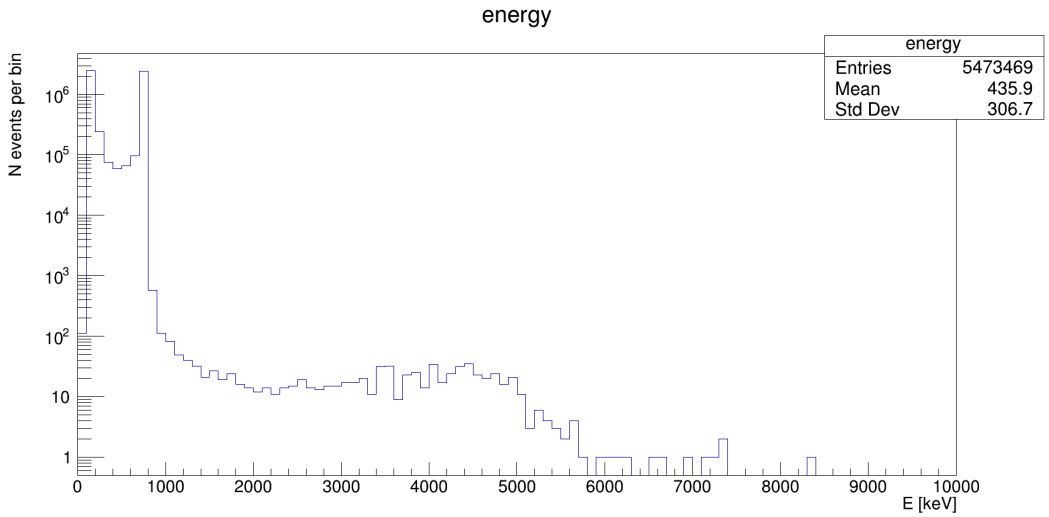

Figure 2.2.1 The original signal measured in the detector chamber with reactor on obtained over 15 days, provided by the νGeN team (image courtesy of K. Smolek).

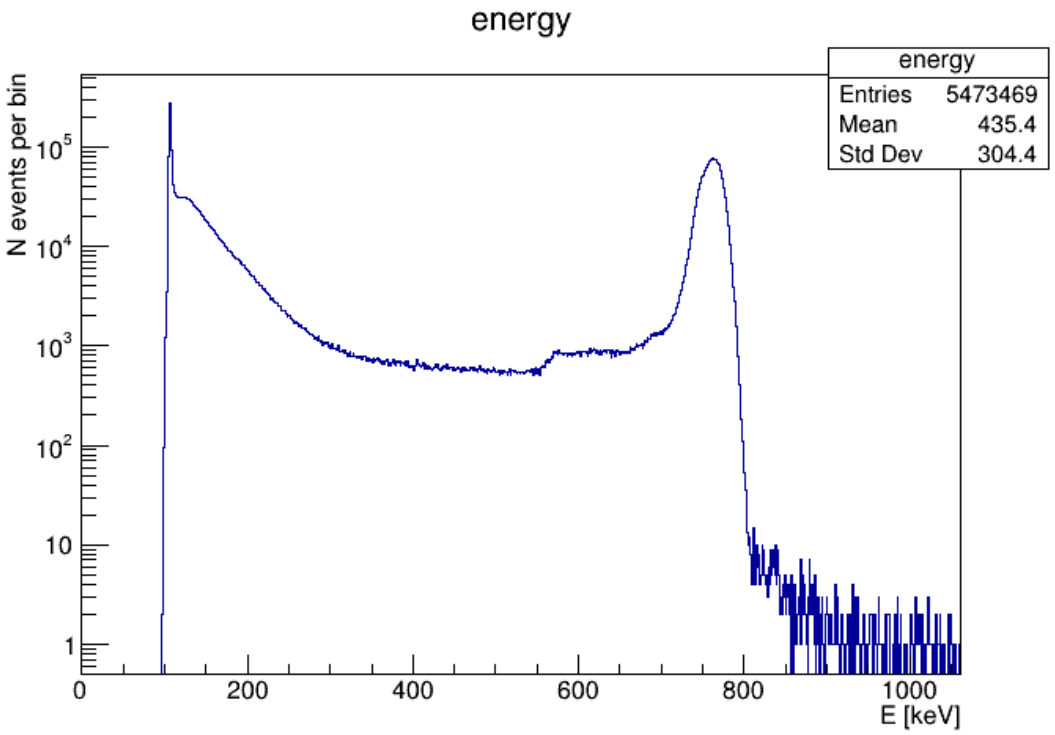

Figure 2.2.2 Detail of the 764 keV peak in the original spectrum (image courtesy of K. Smolek).

Sec. 1.3), their flux was multiplied by six to account for the six sides of the shielding cube – all of them, however, were still sent to the top side of the shielding to simplify the simulation – and directions of their momenta were generated randomly with the restriction that they should point to the half-space containing the experiment. Higher energy neutrons were not multiplied in this way and their momenta were directed perpendicularly to the surface of the shielding to reflect the assumption, that they originate in the reactor and its surroundings, which are located above the experiment in the real setup. All neutrons were generated at the surface of the outermost layer of shielding.

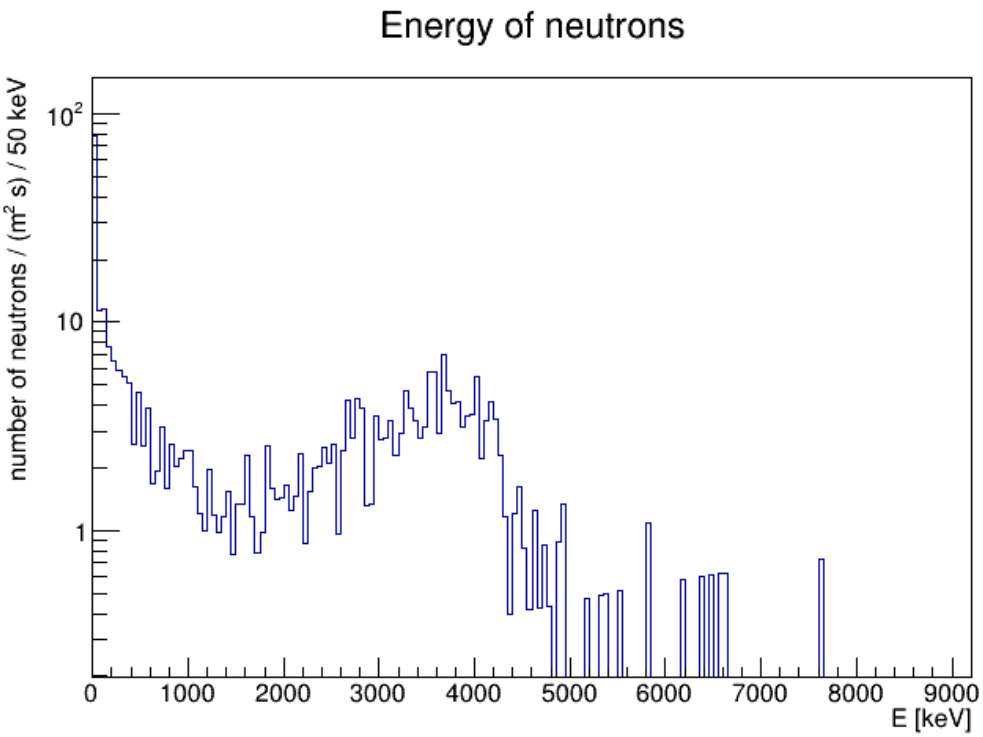

Figure 2.2.3 Deconvoluted spectrum used as an input spectrum for the simulation (image courtesy of K. Smolek).

2.3 Simulation of the neutron background

Following recommendations of colleagues experienced in using GEANT4 for simulating neutrons and of official GEANT4 resources [36, 37], the `QGSP_BERT_HP` reference physics list containing high precision model for simulation of neutrons with energies below 20 MeV was utilized for description of physics processes occurring in the simulation. Primary events were generated based on a spectrum obtained as described in Sec. 2.2. It was loaded from a text file where each line constituted one primary particle and contained its energy, type, momentum direction, starting position and ancestor information to allow for tracing its origin, see below. In each event, a random integer was generated and the appropriate particle from the primary spectrum was selected. Its starting position, energy, type and the direction of its momentum were set by calling the appropriate methods of GEANT4's `G4ParticleGun` object and the event was processed. In each step of the simulation (see Sec. 1.4.1) a check was performed: if the pre-step point and post-step point both lay in the volume of the HPGe crystal, total energy deposited in the step was added to a counter. At the end of each event, content of this counter was written to an output file, along with identification of the primary particle, and it was reset at the start of the next event. Thus the spectrum of deposited energy was obtained.

However, the first runs of the simulation have shown that even for a relatively large number of primary particles (10^7), only a handful of events deposit energy in the detector. Thus to obtain a reasonable statistics, a very large number of events would have to be simulated taking a large amount of time. Hence it was decided to employ a technique called *event biasing* [38]. The principle of this technique is an amplification of so called *rare* events – these would in this case be those that passed all the way to the detector or caused a birth of some other particle which or whose secondaries would reach it. Thence a functionality was added to monitor

the spectrum of particles passing the boundary between two GEANT4 volumes. In each step, a check was performed to find out, whether the currently simulated particle is passing the boundary between two volumes specified at the start of the simulation. An oriented boundary was considered – that is, only particles passing from volume A to volume B were considered, but not those passing from volume B to volume A. For each particle meeting this requirement, its position, energy, type, ancestor information and momentum direction were saved. Particle was then marked as already processed and was ignored if it was seen crossing the boundary again in some future step (for instance if it happened to bounce back to the previous volume and then again crossed into the next one). Only particles, whose direct parent was not marked as seen at the time of their birth, were considered to prevent duplication.

Such a simulation was run for each layer of shielding: always the input spectrum was amplified by a fixed factor $k = 10$, the simulation was executed and both the energy deposited in the detector and the spectrum of particles leaving the given layer for the next one were saved. This spectrum was then used as an input spectrum for the next run – note that the positions of particles were saved as well and were loaded in the next run so that the newly generated particles started from the same position where they were saved in the previous run, that is at the boundary of the two relevant layers of shielding. Thus, in the last run, the spectrum of particles that was previously seen passing from the layer of copper into the layer of nylon was amplified and sent against the layer of nylon, this time saving only the deposited energy. In each run, for each saved particle, information about its ancestor particles was saved. This was then used to attribute their energy deposit to one virtual initial neutron – neutron of the original primary spectrum for the first run of the simulation which *would* produce the secondaries leading to this deposit if no amplification was employed. Sum of these deposits of secondary particles was then taken for each virtual initial neutron to approximate the behavior of a real detector which sees only the total energy deposited by all secondaries, due to its limited time resolution. Spectra of deposited energy obtained in each run were then divided by corresponding amplification coefficients, calculated for the n-th run as $C \cdot k^n$ where

$$C = k_0 \frac{m}{A \cdot 3600 \cdot 24}$$

is a constant scaling the result to counts per day per kilogram of detector mass m (see Sec. 1.2.1), with $k_0 = 100$ being the initial amplification factor. The fact that the area of the top side of the outermost layer of shielding $A \approx 1$ m^2 was included here as well.

3 Results

3.1 Sanity check

Described implementation of the event biasing method (see Sec. 2.3) can also be taken advantage of to check the consistency of the obtained results. Histogram of energy deposits obtained from each run is shown in Fig. 3.1.1. Viewing it, it can be observed that the energy deposit is the same (overlooking some marginal inaccuracy introduced by the probabilistic nature of the processes and low statistics obtained in the first runs) irrespective of on the surface of which volume the primary particles were generated. From this, it can be inferred that the results are consistent and in agreement with the situation where only the initial neutrons were sent against the outermost layer of shielding.

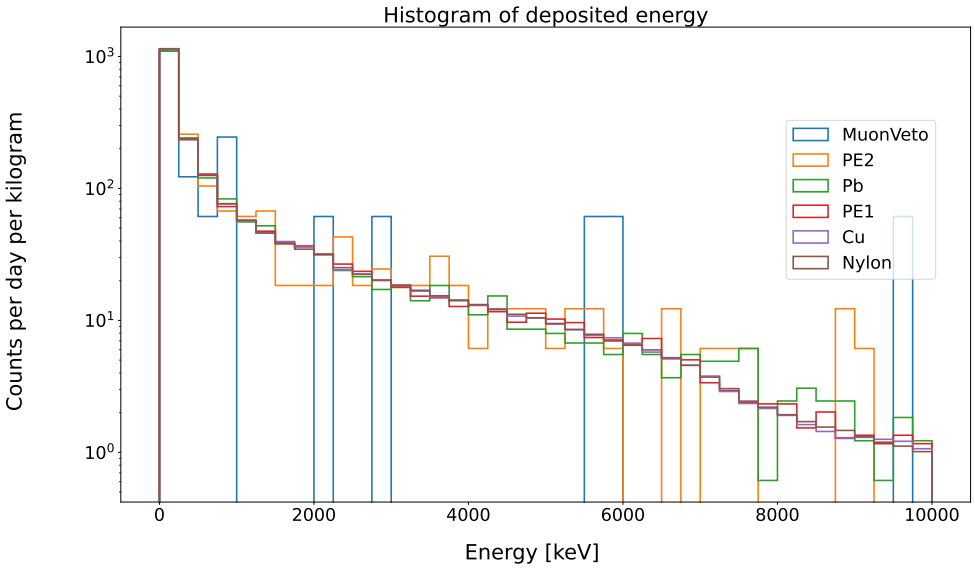

Figure 3.1.1 Histogram of energy deposited in each run – labels correspond to names of GEANT4 volumes on whose outer border the current run generated primaries.

Furthermore, upon viewing the neutron and gamma spectra entering each volume plotted in figure Fig. 3.1.2, it can be stated that the number of neutrons decreases as they near the detector. Similar can be said about the gamma spectra, where significant decrease occurs in lead. Moreover, some anticipated peaks can be identified in the latter, such as the peak at 2.2 MeV caused by the neutron capture on hydrogen or 0.48 MeV peak caused by the boron admixture (cf. Sec. 1.3), suggesting that physics processes relevant for the simulation are implemented correctly in the utilized physics list and that the simulation runs in accordance with physical reality.

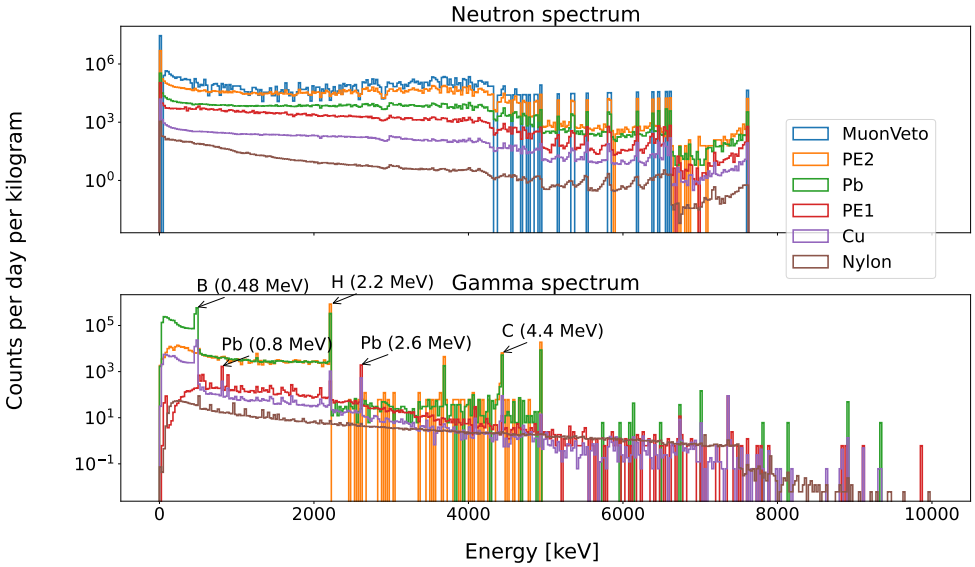

Figure 3.1.2 Neutron and gamma spectra entering each run of the simulation.

3.2 Analysis and discussion[6]

Comparison of the simulated background with the reactor on with the expected CEνNS signal calculated by the νGeN team [2] based on Eq. (1.1.2) is plotted in Fig. 3.2.1 for the low energy region. Special attention has been paid to the deposited energy spectrum in the region of interest (ROI) indicated by the first measurements of νGeN (see Sec. 1.2.2). A histogram of the energy deposit in this region is shown in Fig. 3.2.2. Summing all the bins, a value of 4.61 ± 0.05 events per day per kilogram is obtained[7]. Comparing this to the value obtained from the first measurements of νGeN (see Sec. 1.2.2), it can be observed that it's approximately double, well within the standard deviation, which is a good but also interesting agreement considering the approximations made and especially the uncertainty in the initial neutron spectrum. At the same time, because of the multiplication of the flux of thermal neutrons by the factor of six (see Sec. 2.2), this should be (again, within the reliability limit of the initial spectrum, which will not be assessed here) an upper estimate of the neutron background influence. To get the lower estimate, the simulation was rerun without applying such multiplication. This yielded the histogram shown in Fig. 3.2.3, the sum being 4.65 ± 0.05 events per day per kilogram. The effect of thermal neutrons is thus negligible. In fact, in the region of interest, they have no influence on the data at all, which can be seen from a two dimensional histogram putting the energy of the initial neutron on the x-axis and the energy deposited in the event on the y-axis, see Fig. 3.2.4[8]. The energy deposit in the ROI is contributed solely by neutrons with higher energies.

[6] All data presented in this section come from the last run of the simulation, that is the primary particles were generated on the surface of the layer of nylon based on the spectrum of particles reaching it in the previous run.

[7] For each bin, the standard deviation was taken to be the square root of the number of events in the given bin as a first approximation of the standard deviation of the Poisson distribution. The standard deviation of the total count was then calculated as the square root of the sum of second powers of these deviations. Afterwards, the result was divided by the amplification coefficient.

[8] Note: the counts are not scaled to day and kilogram of detector mass, as the purpose of the plot is a relative comparison of influence of various energies possessed by the initial neutron.

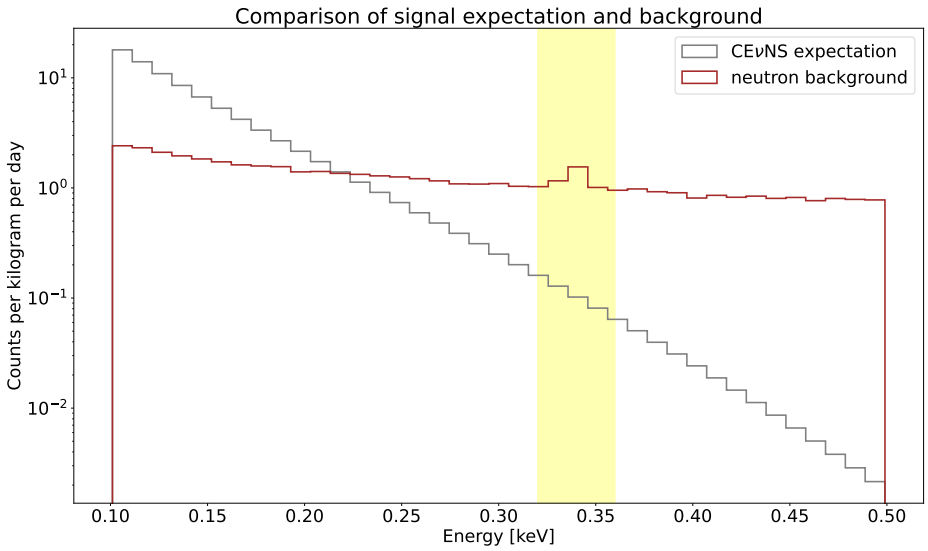

Figure 3.2.1 Comparison of the simulated background with the reactor on and the expected CEνNS signal plotted for quenching factor 0.179 in the low energy range with highlighted ROI.

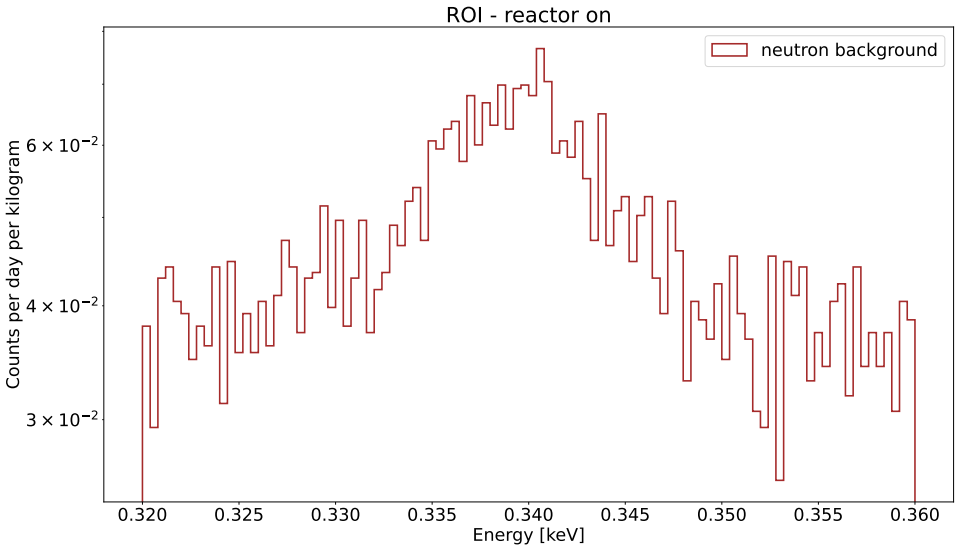

Figure 3.2.2 Deposited energy in ROI with the flux of thermal neutrons multiplied by six.

For comparison, same process as described in Sec. 2.3 was applied to the initial neutron spectrum with the reactor off which was again deconvoluted as described in Sec. 2.2 with the result plotted in Fig. 3.2.5. As can be seen from comparison with Fig. 2.2.3, the most significant difference is in the low energy region under 1 MeV and especially in the flux of thermal neutrons – the flux of thermal neutrons is only 0.58 neutrons per $m^2 \cdot s$ here, while the flux of non-thermal neutrons is 212 neutrons per $m^2 \cdot s$. The observation made from the 2D histogram would thus suggest that there will not be any significant difference in the spectrum of deposited energy in the ROI contributed by the neutron background. Indeed, repeating the simulation with this spectrum (again with the flux

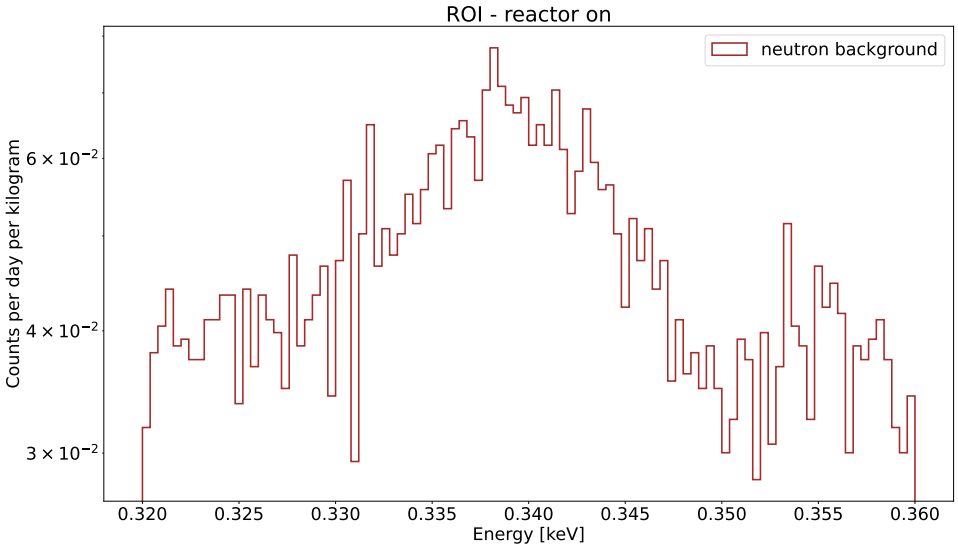

Figure 3.2.3 Deposited energy in ROI without the multiplication factor of thermal neutrons.

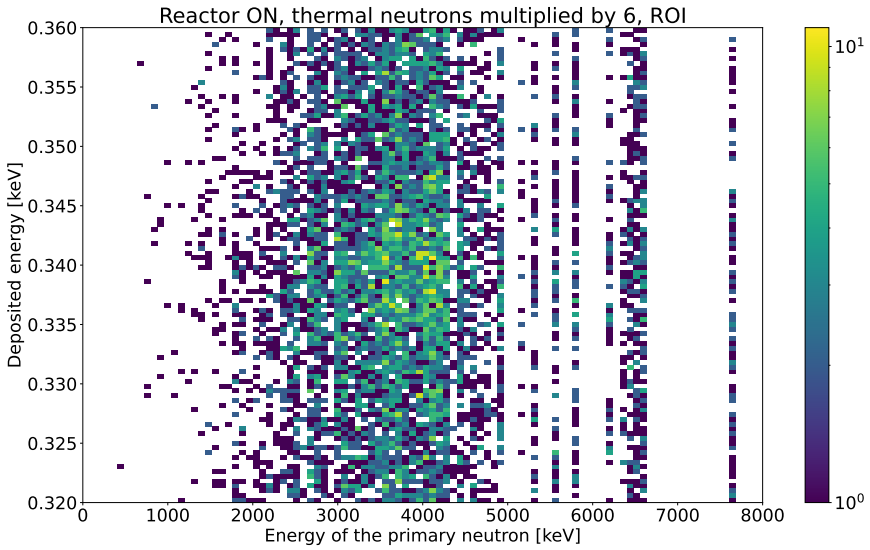

Figure 3.2.4 2D histogram showing the dependence of the deposited energy on the energy of primary neutron for reactor on and initial number of thermal neutrons multiplied by six.

of thermal neutrons amplified by the factor of 6) taken as the source of initial primaries, the histogram shown in Fig. 3.2.6 is obtained. Here the total number of events is 5.19 ± 0.06 events per day per kilogram.

Curiously, this is more than when the initial spectrum for reactor on is used. To better understand this peculiarity, the evolution of the neutron (Fig. 3.2.7) and gamma (Fig. 3.2.8) spectra[9] across the layers of shielding must be consulted. These show that while the total initial flux of neutrons is greater with the reactor on, this difference is most prominently contributed by the low energy part of

[9] Again, as the comparison here is relative, the histograms were not scaled to any particular time interval and are left as they were obtained from the simulation with the amplified input spectrum.

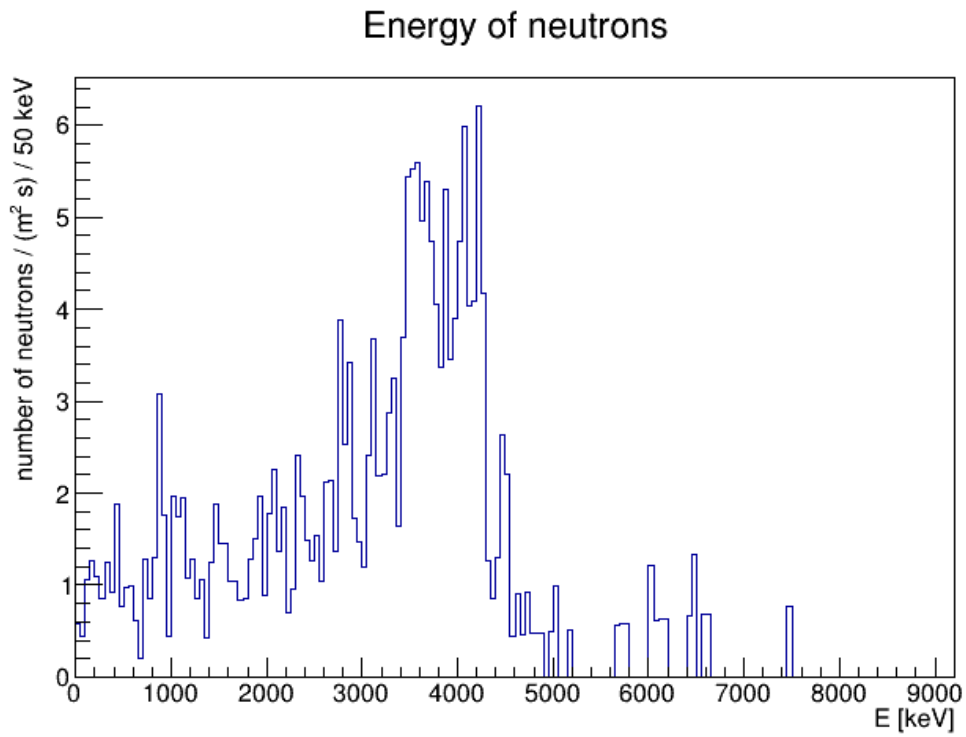

Figure 3.2.5 Input spectrum of neutrons with the reactor off (image courtesy of K. Smolek).

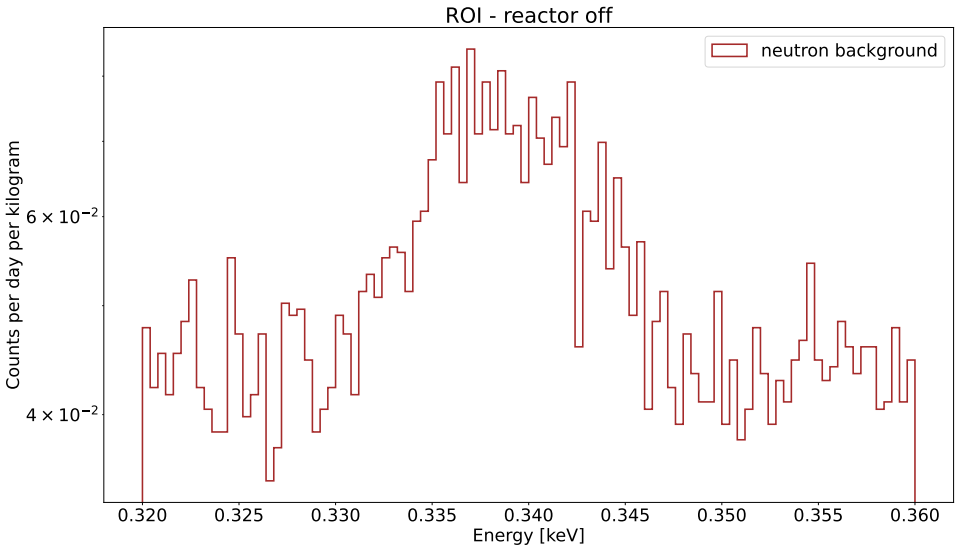

Figure 3.2.6 Deposited energy in the ROI with the reactor off and with the flux of thermal neutrons multiplied by the factor of six.

the spectrum, while at higher energies over 4 MeV, the flux with the reactor off is slightly greater. The former leads to the generation of many more gamma photons in the first hydrogenous layers of shielding in the case of the reactor on, however this difference is evened out after the particles pass through the layer of lead. There on the other hand the abundance of higher energy neutrons in the spectrum with the reactor off finally fully manifests itself and leads to the spectrum of gamma photons with the reactor off to overtake the one with the

reactor on. The neutron spectrum then remains similar for the both states of the reactor with the off state being slightly dominant in the higher energies. This is then propagated to the lower energies as well by the layer of copper. Thus indeed the slight difference in the higher energy part of the initial neutron spectra seems to result in higher event rate for reactor off, while the difference in low energy neutrons under approximately 1 MeV is lost as they pass through the shielding.

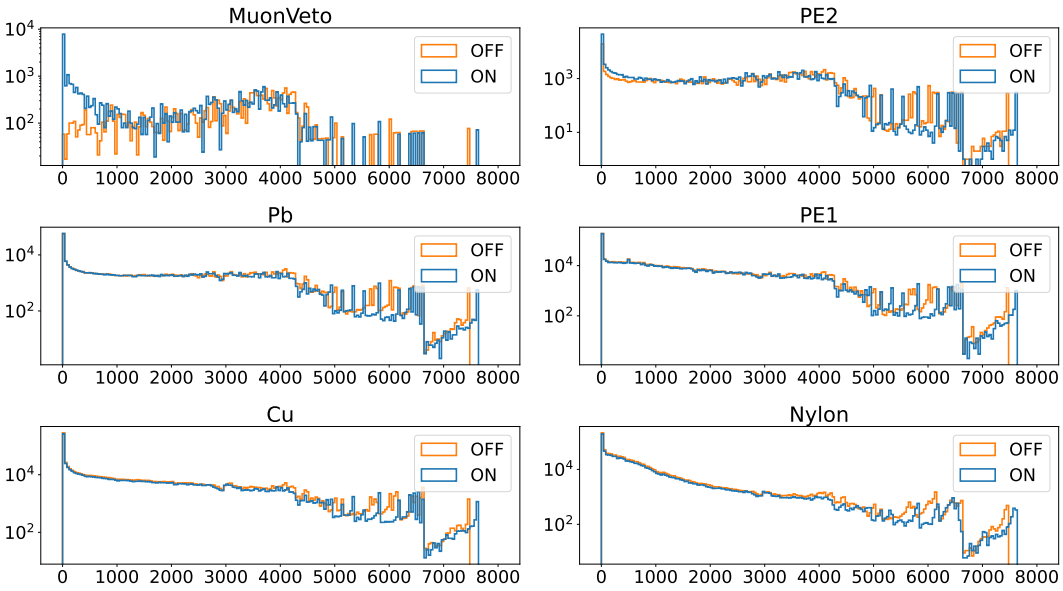

Figure 3.2.7 Evolution of the neutron spectrum across layers of shielding for the two states of the reactor (no amplification of the thermal neutrons flux was made).

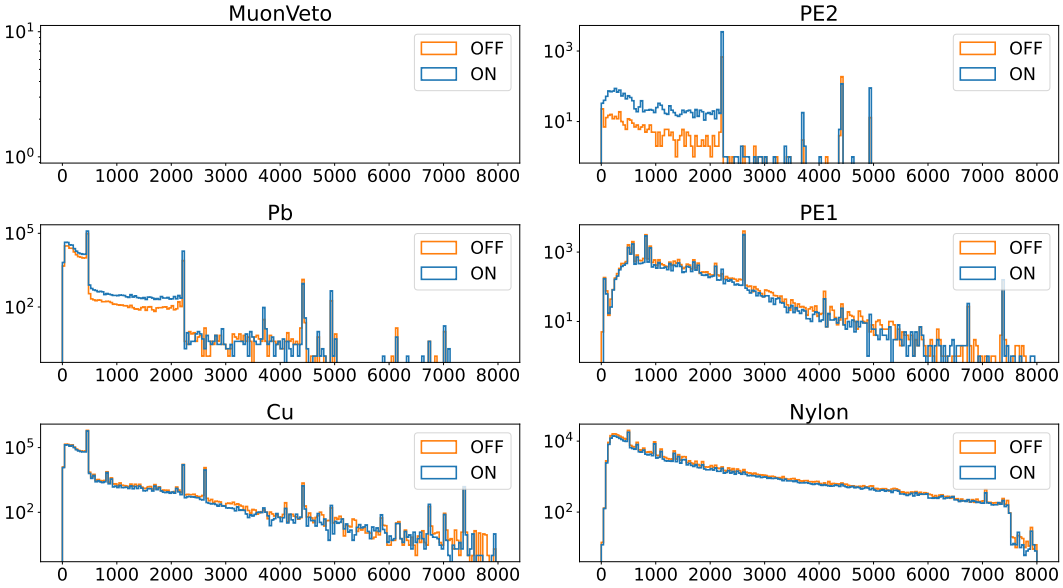

Figure 3.2.8 Evolution of the gamma spectrum across layers of shielding for the two states of the reactor (without the amplification of the thermal neutron flux).

It however remains to assess and explain what causes the difference in the flux at higher energies. One satisfactory answer is that the input spectrum was not

unfolded adequately and that more careful analysis will reveal that the difference is negligible – the low statistics in the high energy region leads to a great error in the flux estimate. The other possibility is that some processes which were not considered take place in the reactor when it is turned off, such as decay of some products of the nuclear reaction occurring within which do not present themselves as prominently when the reactor is running, and so truly the flux is greater in the high energy range with the reactor off. Clearly some decay still occurs in the reactor after it's switched off, otherwise no flux would be seen then. It would also be worth investigating whether some mechanisms which reduce the neutron flux when the reactor is running might be turned off along with the reactor.

Conclusion

A Monte-Carlo simulation of the neutron background in the νGeN experiment focused on the detection of the CEνNS was performed using the GEANT4 simulation framework and the output was compared to the expected CEνNS signal in the region of interest and to the actual measured data. Presented results indicate that it's possible that the signal observed during the first measurements of the experiment was caused solely by neutrons. This is supported by the fact that no difference in event rate was observed by the experiment within the bounds of the standard deviation. Also it was discovered that thermal neutrons have no effect on the signal in the region of interest. There, higher event rate was obtained when the initial spectrum of neutrons with the reactor off was considered than for the initial spectrum with the reactor on. Discussion of these effects was carried out and suggestions were presented for their explanation.

To further assess the problem of the influence of the neutron background and obtain more precise results, several steps can be taken. Most importantly, the input neutron spectrum should be reevaluated and a more precise estimate should be made, where the sensitivity and responsivity of the ^{3}He detector which was used for its measurement and also the spatial setup of the measurement will be taken into account more delicately. A more sophisticated approach should also be applied to the unfolding procedure of the spectrum. Also, an attempt to better understand the difference in the neutron spectra with the reactor off and on should be made, especially in the region of thermal neutrons where it is most significant, as the reason for it is still unclear and the answer might suggest some other implications for the experiment.

Regarding the simulation itself, better accuracy of results could be achieved if even more events were simulated, choosing greater amplification factor k. Also, a better approach could be chosen with respect to the directions of the momenta of the initial non-thermal neutrons – some sort of method for generation of random direction vectors could be devised which would however have bias in one direction to reflect the assumptions that the neutrons measured around the experiment come from the reactor above it and its surroundings.

References

[1] Belov, V. et al. The νGeN experiment at the Kalinin Nuclear Power Plant. *Journal of Instrumentation*. IOP Publishing, dec, 2015, Vol. 10, No. 12, pp. P12011–P12011. Available from DOI 10.1088/1748-0221/10/12/p12011. Available from https://doi.org/10.1088/1748-0221/10/12/p12011.

[2] Alekseev, I. et al. *First results of the nuGeN experiment on coherent elastic neutrino-nucleus scattering*. Available from DOI 10.48550/ARXIV.2205.04305. Available from https://arxiv.org/abs/2205.04305.

[3] Laboratory, Fermi National Accelerator. *All Things Neutrino*. Available from https://neutrinos.fnal.gov/. Accessed on 2022-02-23 and 2022-04-19.

[4] Griffiths, David. *Introduction to Elementary Particles*. John Wiley & Sons, Inc., 1987. ISBN 0-471-60386-4.

[5] Aker, M. et al. Direct neutrino-mass measurement with sub-electronvolt sensitivity. *Nature Physics*. Feb, 2022, Vol. 18, No. 2, pp. 160-166. ISSN 1745-2481. Available from DOI 10.1038/s41567-021-01463-1. Available from https://doi.org/10.1038/s41567-021-01463-1.

[6] Pontecorvo, Bruno. Mesonium and Antimesonium. *Soviet Journal of Experimental and Theoretical Physics*. 1958. Available from https://ui.adsabs.harvard.edu/abs/1958JETP....6..429P.

[7] Pontecorvo, Bruno. Neutrino Experiments and the Problem of Conservation of Leptonic Charge. *Soviet Journal of Experimental and Theoretical Physics*. May, 1958. Available from https://ui.adsabs.harvard.edu/abs/1968JETP...26..984P.

[8] Fukuda, Y. et al. Evidence for Oscillation of Atmospheric Neutrinos. *Phys. Rev. Lett.* American Physical Society, Aug, 1998, Vol. 81, pp. 1562–1567. Available from DOI 10.1103/PhysRevLett.81.1562. Available from https://link.aps.org/doi/10.1103/PhysRevLett.81.1562.

[9] Ahmad, Q. R. et al. Measurement of the Rate of $\nu_e + d \rightarrow p + p + e^-$ Interactions Produced by ^8B Solar Neutrinos at the Sudbury Neutrino Observatory. *Phys. Rev. Lett.* American Physical Society, Jul, 2001, Vol. 87, pp. 071301. Available from DOI 10.1103/PhysRevLett.87.071301. Available from https://link.aps.org/doi/10.1103/PhysRevLett.87.071301.

[10] Cowan, C. L. et al. Detection of the Free Neutrino: a Confirmation. *Science*. 1956, Vol. 124, No. 3212, pp. 103-104. Available from DOI 10.1126/science.124.3212.103. Available from https://www.science.org/doi/abs/10.1126/science.124.3212.103.

[11] Mention, G. et al. Reactor antineutrino anomaly. *Physical Review D*. American Physical Society (APS), apr, 2011, Vol. 83, No. 7. Available from DOI 10.1103/physrevd.83.073006. Available from https://doi.org/10.1103%2Fphysrevd.83.073006.

[12] Alekseev, I. et al. Search for sterile neutrinos at the DANSS experiment. *Physics Letters B*. Elsevier BV , dec, 2018, Vol. 787, pp. 56–63. Available

from DOI 10.1016/j.physletb.2018.10.038. Available from https://doi.org/10.1016%2Fj.physletb.2018.10.038.

[13] *COHERENT*. Available from https://coherent.ornl.gov. Accessed on 2021-02-21.

[14] Freedman, Daniel Z. Coherent effects of a weak neutral current. *Phys. Rev. D*. American Physical Society, Mar, 1974, Vol. 9, pp. 1389–1392. Available from DOI 10.1103/PhysRevD.9.1389. Available from https://link.aps.org/doi/10.1103/PhysRevD.9.1389.

[15] Anderson, A. J. et al. Coherent neutrino scattering in dark matter detectors. *Physical Review D*. American Physical Society (APS), jul, 2011, Vol. 84, No. 1. Available from DOI 10.1103/physrevd.84.013008. Available from https://doi.org/10.1103%2Fphysrevd.84.013008.

[16] Akimov, D. et al. Observation of coherent elastic neutrino-nucleus scattering. *Science*. 2017, Vol. 357, No. 6356, pp. 1123-1126. Available from DOI 10.1126/science.aao0990. Available from https://www.science.org/doi/abs/10.1126/science.aao0990.

[17] *Joint Institute for Nuclear Research*. Available from http://www.jinr.ru/about-en/. Accessed on 24-02-2022.

[18] *Mirion Technologies, Inc. Radiation Measurement & Detection Devices*. Available from https://www.mirion.com/.

[19] Chadwick, J. Possible Existence of a Neutron. *Nature*. Feb, 1932, Vol. 129, No. 3252, pp. 312–312. ISSN 1476-4687. Available from DOI 10.1038/129312a0. Available from https://doi.org/10.1038/129312a0.

[20] *Interaction of neutrons with matter*. Available from https://www.nrc.gov/docs/ML1122/ML11229A705.pdf.

[21] *Interaction of radiation with matter – Interaction of neutrons with matter*. Available from https://courses.grainger.illinois.edu/npre441/sp2020/lctr%20notes/lecture_chapter4_2020_interaction_neutrons.pdf.

[22] *Neutron Flux Spectra*. Available from https://www.nuclear-power.com/nuclear-power/reactor-physics/nuclear-engineering-fundamentals/neutron-nuclear-reactions/neutron-flux-spectra/. Accessed on 2022-05-04.

[23] Panikkath, Priyada et al. Estimation of neutron energy distributions from measured prompt gamma intensities: Experimental validation. *Nuclear Instruments and Methods in Physics Research Section A: Accelerators, Spectrometers, Detectors and Associated Equipment*. 2020, Vol. 969, pp. 164101. ISSN 0168-9002. Available from DOI https://doi.org/10.1016/j.nima.2020.164101. Available from https://www.sciencedirect.com/science/article/pii/S0168900220305052.

[24] *Boron - Protons - Neutrons - Electrons - Electron Configuration*. Available from https://material-properties.org/Boron-protons-neutrons-electrons-electron-configuration/. Accessed on 2022-05-01.

[25] *Shielding of Gamma Radiation | Types & Uses | nuclear-power.com*. Available from https://www.nuclear-power.com/nuclear-power/reactor-physics/atomic-nuclear-physics/radiation/shielding-of-ionizing-radiation/shielding-gamma-radiation/. Accessed on 2022-05-01.

[26] *Overview*. Available from https://geant4.web.cern.ch/. Accessed on 2022-02-28.

[27] AGOSTINELLI, S. et al. Geant4—a simulation toolkit. *Nuclear Instruments and Methods in Physics Research Section A: Accelerators, Spectrometers, Detectors and Associated Equipment*. 2003, Vol. 506, No. 3, pp. 250-303. ISSN 0168-9002. Available from DOI https://doi.org/10.1016/S0168-9002(03)01368-8. Available from https://www.sciencedirect.com/science/article/pii/S0168900203013688.

[28] ALLISON, J. et al. Recent developments in Geant4. *Nuclear Instruments and Methods in Physics Research Section A: Accelerators, Spectrometers, Detectors and Associated Equipment*. 2016, Vol. 835, pp. 186-225. ISSN 0168-9002. Available from DOI https://doi.org/10.1016/j.nima.2016.06.125. Available from https://www.sciencedirect.com/science/article/pii/S0168900216306957.

[29] *Monte Carlo method*. Available from https://en.wikipedia.org/wiki/Monte_Carlo_method. Accessed on 2022-05-01.

[30] *About ROOT*. Available from https://root.cern/about/. Accessed on 2022-04-06.

[31] ARCHAMBAULT, S. et al. Optimization of Neutron Shielding for the PICASSO Experiment. *AIP Conference Proceedings*. 2009, Vol. 1180, No. 1, pp. 112-116. Available from DOI 10.1063/1.3266086. Available from https://aip.scitation.org/doi/abs/10.1063/1.3266086.

[32] *Wikipedia*. Available from en.wikipedia.org. Accessed on 2022-05-04.

[33] ROZOV, S. et al. *Monitoring of the thermal neutron flux in the LSM underground laboratory*. Available from DOI 10.48550/ARXIV.1001.4383. Available from https://arxiv.org/abs/1001.4383.

[34] *Laboratoire souterrain de Modane*. Available from http://www.lsm.fr/.

[35] *Brookhaven National Laboratory, National Nuclear Data Center – Sigma Periodic Table Browse*. Available from https://www.nndc.bnl.gov/sigma/index.jsp.

[36] *Use Cases - Reference Physics Lists*. Available from https://geant4.web.cern.ch/node/302. Accessed on 2022-05-05.

[37] *Reference Physics Lists*. Available from https://geant4.web.cern.ch/node/155. Accessed on 2022-05-05.

[38] VERDERI, Marc. *Biasing in* GEANT4. Available from https://indico.cern.ch/event/746466/contributions/3345717/attachments/1833991/3004166/biasing.pdf. Accessed on 2022-05-06.